

Numerical solution for multiple confocal elliptic dissimilar cylinders

Y. Z. Chen*

Division of Engineering Mechanics, Jiangsu University, Zhenjiang, Jiangsu, 212013, P.R. China

(Received February 16, 2016, Revised November 29, 2016, Accepted November 30, 2016)

Abstract. This paper provides a numerical solution for multiple confocal elliptic dissimilar cylinders. In the problem, the inner elliptic notch is under the traction free condition. The medium is composed of many confocal elliptic dissimilar cylinders. The transfer matrix method is used to study the continuity condition for the stress and displacement along the interfaces. Two cases, or the infinite matrix case and the finite matrix case, are studied in this paper. In the former case, the remote tension is applied in y -direction. In the latter case, the normal loading is applied along the exterior elliptic contour. For two cases, several numerical results are provided.

Keywords: confocal elliptic dissimilar cylinders; stress concentration factor; complex variable method; transfer matrix method

1. Introduction

The stress analysis for the elliptic inclusions, the elliptic inhomogeneities, the elliptic confocal layers in plane elasticity or antiplane elasticity received much attention by many researchers (Gong 1995, Chen 2004, Chen 2013, Chen and Wu 2007, Zhu *et al.* 2013, Wu and Chen 1990, Wang and Gao 2011, Chen 2015a,b). In the case of plane elasticity, it is a general way to use the conformal mapping technique. The elliptic confocal layer is mapped into a ring region. The complex potentials are expanded into a Laurent series. However, the continuity conditions along the interface are the inherent difficulties in the analysis. This paper aims to overcome the mentioned difficulties.

Several relevant references are introduced below. A generalized and unified treatment was presented for the antiplane problem of elastic elliptical inclusion undergoing uniform eigenstrains and subjected to arbitrary loading in the surrounding matrix (Gong 1995). The problem of a confocally multicoated elliptical inclusion in an unbounded matrix subjected to an antiplane shear was studied (Chen 2004). A closed form solution was provided for the Eshelby's elliptic inclusion in antiplane elasticity (Chen 2013). In the formulation, the prescribed eigenstrains are not only for the uniform distribution, but also for the linear form. The null-field integral equation for an infinite medium containing circular holes and/or inclusions was derived (Chen and Wu 2007). A comprehensive survey of recent works on inclusion was provided (Zhu *et al.* 2013). The problems of multiple inclusions, dislocations and cracks as well as various methods used to study these problems were discussed.

The plane and antiplane problems associated with a crack in a confocal elliptic inhomogeneity embedded in an infinite medium was solved in detail (Wu and Chen 1990). Particularly, the dependence of the stress intensity on the size of the inhomogeneity was examined. The stress field inside a two-dimensional arbitrary-shape elastic inclusion bonded through an interphase layer to an infinite elastic matrix subjected to uniform stresses at infinity was analytically studied using the complex variable method in elasticity (Wang and Gao 2011).

Previously, the problem for multiply confocal layers with dissimilar elastic properties were studied (Chen 2015a). In that paper, the continuity conditions for the displacement and stress along interface were reduced to a relation between two sets of the coefficients in the Laurent series for the complex potentials for two adjacent layers of the interface. This relation can be expressed in the form of a transfer matrix. This method or the transfer matrix method can considerably reduce the work for derivation and computation. For example, this method can be used easily to the case of multiply confocal layers. The derivation and the formulation were based on the fact that all material property constants, or G_j (shear modulus) κ_j ($j=1,2,\dots$) must not be equal to zero, or $G_j \neq 0$ and $\kappa_j \neq 0$ ($j=1,2,\dots$). In the present paper, we assume G and κ values to be equal to zero for the portion interior to the inner elliptic contour. It is seen that the problem studied in the present paper has some difference with the paper (Chen 2015a).

Two and three-dimensional analytical solutions for an inhomogeneity annulus/ring with eigenstrain are presented (Markenscoff and Dundurs 2014). Since the shapes studied in this paper are the confocal elliptic layers, the technique used for the annular region in (Markenscoff and Dundurs 2014) cannot be directly used to the present paper.

A novel solution for thick-walled cylinders made of

*Corresponding author, Professor
E-mail: chens@ujs.edu.cn

functionally graded materials (FGMs) was provided (Chen 2015b). In the formulation, the cylinder is divided into N layers. On the individual layer, the Young's modulus is assumed to be a constant. For an individual layer, two undetermined constants are involved in the elastic solution. Those undetermined coefficients can be evaluated from the continuation condition along interfaces of layers and the boundary conditions at the inner surface and outer surface of cylinder. The suggested method is similar to the transfer matrix method in this paper.

This paper provides a stress analysis for multiple confocal elliptic dissimilar cylinders. In the problem, the inner elliptic notch is under the traction free condition. The medium is composed of many confocal elliptic dissimilar cylinders. The conformal mapping method is used in the paper thoroughly. The complex potentials are expressed in the form of the Laurent series in the ring region. The transfer matrix method is used to study the continuity condition for the stress and displacement along the interfaces. Two cases, or the infinite matrix and the finite matrix, are studied in this paper. In the former case, the remote tension is applied in y - direction. In the latter case, the normal loading is applied along the exterior elliptic contour. For two cases, several numerical results are provided.

2. Analysis

2.1 Some basic equations in complex variable method in plane elasticity

The following analysis depends on the complex variable function method in plane elasticity (Muskhelishvili 1963). In the method, the stresses ($\sigma_x, \sigma_y, \sigma_{xy}$), the resultant forces (X, Y) and the displacements (u, v) are expressed in terms of two complex potentials $\phi_*(z)$ and $\psi_*(z)$ such that

$$\sigma_x + \sigma_y = 4 \operatorname{Re} \phi_*'(z) \quad (1)$$

$$\sigma_y - \sigma_x + 2i\sigma_{xy} = 2[\bar{z}\phi_*''(z) + \psi_*'(z)]$$

$$F = -Y + iX = \phi_*(z) + z\overline{\phi_*'(z)} + \overline{\psi_*(z)} \quad (2)$$

$$2G(u + iv) = \kappa\phi_*(z) - z\overline{\phi_*'(z)} - \overline{\psi_*(z)} \quad (3)$$

where $z=x+iy$ denotes complex variable, G is the shear modulus of elasticity, $\kappa = (3 - \nu)/(1 + \nu)$ is for the plane stress problems, $\kappa = 3 - 4\nu$ is for the plane strain problems, and ν is the Poisson's ratio. In the present study, the plane strain condition is assumed thoroughly. In the following, we occasionally rewrite the displacements "u", "v" as u_1, u_2 , $\sigma_x, \sigma_y, \sigma_{xy}$ as $\sigma_{11}, \sigma_{22}, \sigma_{12}$, and "x", "y" as X_1, X_2 , respectively.

In the analysis, we use the following conformal

mapping (Muskhelishvili 1963) (Fig. 1)

$$z = \omega(\zeta) = R\left(\zeta + \frac{m}{\zeta}\right), \quad (R = \frac{a+b}{2}, \quad m = \frac{a-b}{a+b}) \quad (4)$$

$$\omega'(\zeta) = R\left(1 - \frac{m}{\zeta^2}\right), \quad \omega''(\zeta) = \frac{2Rm}{\zeta^3} \quad (5)$$

In Eq. (4), R and m , or a and b , are given beforehand.

The inversion of the mapping function $z = \omega(\zeta)$ is defined by

$$\zeta = \Omega(z) = \frac{z + \sqrt{z^2 - 4mR^2}}{2R} \quad (6)$$

In the following analysis, we denote

$$\phi(\zeta) = \phi_*(z) \Big|_{z=\omega(\zeta)}, \quad \psi(\zeta) = \psi_*(z) \Big|_{z=\omega(\zeta)} \quad (7)$$

Clearly, after using the mentioned conformal mapping, from Eqs. (1) to (3) we have

$$\sigma_x + \sigma_y = 4 \operatorname{Re} \frac{\phi'(\zeta)}{\omega'(\zeta)} \quad (8)$$

$$\sigma_y - \sigma_x + 2i\sigma_{xy} = 2 \left(\frac{\overline{\omega(\zeta)} (\phi''(\zeta)\omega'(\zeta) - \phi'(\zeta)\omega''(\zeta))}{(\omega'(\zeta))^3} + \frac{\psi'(\zeta)}{\omega'(\zeta)} \right)$$

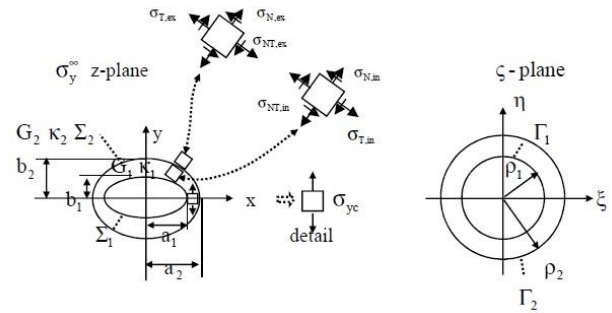


Fig. 1 Mapping relations: (1) the elliptic layer bounded by two ellipses Σ_1 (with two semi-axes "a₁" and "b₁"), and Σ_2 (with two semi-axes "a₂" and "b₂" and $\sqrt{a_2^2 - b_2^2} = \sqrt{a_1^2 - b_1^2}$), (in the z -plane) with elastic constants G_1, κ_1 mapped into ring region bounded by two circles Γ_1 and Γ_2 , or $\rho_1 \leq |\zeta| \leq \rho_2$ with $\rho_1 = 1$ (in the ζ -plane), (2) the infinite matrix region exterior to the interface Σ_2 (in the z -plane) with elastic constants G_2, κ_2 mapped into the infinite region exterior to circle Γ_2 , or $|\zeta| \geq \rho_2$ (in the ζ -plane)

$$F = -Y + iX = \phi(\zeta) + \omega(\zeta) \frac{\overline{\phi'(\zeta)}}{\omega'(\zeta)} + \overline{\psi(\zeta)} \quad (9)$$

$$2G(u + iv) = \kappa\phi(\zeta) - \omega(\zeta) \frac{\overline{\phi'(\zeta)}}{\omega'(\zeta)} - \overline{\psi(\zeta)} \quad (10)$$

From Eqs. (8) to (10) we see that, if one obtains the complex potentials $\phi(\zeta)$ and $\psi(\zeta)$ in the mapping plane, one can get the stress and displacement in the physical plane.

2.2 Formulation of the problem in the infinite matrix case

In the study, the whole region is composed of two phase composites: (1) the elliptic layer bounded by the confocal elliptic layers Σ_1 and Σ_2 with the semi-axes (a_1, b_1) , and semi-axes (a_2, b_2) , respectively and with the elastic constants G_1, κ_1 , (2) the infinite matrix exterior to the interface Σ_2 with the elastic constants G_2, κ_2 (Fig. 1). The remote loading is denoted by $\sigma_y^\infty = p$.

In the formulation, we use the following mapping function (Muskhelishvili 1963)

$$z = \omega(\zeta) = R\left(\zeta + \frac{m}{\zeta}\right), \quad \left(R = \frac{a_1 + b_1}{2}, \quad m = \frac{a_1 - b_1}{a_1 + b_1}\right) \quad (11)$$

In the mapping relation defined by Eq. (11), the elliptic contour Σ_1 (with two semi-axes “ a_1 ” and “ b_1 ”) maps into the unit circle Γ_1 (with $\zeta = \rho_1 e^{i\theta}$, $\rho_1 = 1$). In addition, the elliptic contour Σ_2 (with two semi-axes “ a_2 ” and “ b_2 ”) maps into the circle Γ_2 (with $\zeta = \rho_2 e^{i\theta}$, $\rho_2 > \rho_1$). Clearly, it is easy to prove the following relation $\sqrt{a_2^2 - b_2^2} = \sqrt{a_1^2 - b_1^2}$.

For the region bounded by elliptic contours Σ_1 and Σ_2 , we can define two complex potentials $\phi_*^{(1)}(z)$ and $\psi_*^{(1)}(z)$ (Fig. 1). After using conformal mapping shown by Eq. (11), we can define the relevant complex potentials in the mapping plane as follows

$$\begin{aligned} \phi^{(1)}(\zeta) &= \phi_*^{(1)}(z) \Big|_{z=\omega(\zeta)}, \\ \psi^{(1)}(\zeta) &= \psi_*^{(1)}(z) \Big|_{z=\omega(\zeta)}, \end{aligned} \quad (12)$$

$$(\rho_1 \leq |\zeta| \leq \rho_2, \text{ with } \rho_1 = 1)$$

In the case of symmetric loading, two complex potentials can be expressed in the following Laurent series

form

$$\begin{aligned} \phi^{(1)}(\zeta) &= \sum_{k=-(N-1)}^N a_k^{(1)} \zeta^{2k-1}, \\ \psi^{(1)}(\zeta) &= \sum_{k=-(N-1)}^N b_k^{(1)} \zeta^{2k-1}, \quad (\rho_1 \leq |\zeta| \leq \rho_2) \end{aligned} \quad (13)$$

In Eq. (13), “ N ” denotes the number of terms truncated. Similarly, for the region exterior to the elliptic contour Σ_2 , we can define two complex potentials $\phi_*^{(2)}(z)$ and $\psi_*^{(2)}(z)$. After using conformal mapping shown by Eq. (11), we can define the relevant complex potentials in the mapping plane as follows

$$\begin{aligned} \phi^{(2)}(\zeta) &= \phi_*^{(2)}(z) \Big|_{z=\omega(\zeta)}, \\ \psi^{(2)}(\zeta) &= \psi_*^{(2)}(z) \Big|_{z=\omega(\zeta)}, \quad (|\zeta| \geq \rho_2) \end{aligned} \quad (14)$$

In addition, two complex potentials can be expressed in the following Laurent series form

$$\begin{aligned} \phi^{(2)}(\zeta) &= \sum_{k=-(N-1)}^N a_k^{(2)} \zeta^{2k-1}, \\ \psi^{(2)}(\zeta) &= \sum_{k=-(N-1)}^N b_k^{(2)} \zeta^{2k-1}, \quad (|\zeta| \geq \rho_2) \end{aligned} \quad (15)$$

It is known that, in the case of remote loading σ_y^∞ , two complex potentials $\phi_*^{(2)}(z)$ and $\psi_*^{(2)}(z)$ can be expanded in the following series form (Muskhelishvili 1963)

$$\begin{aligned} \phi_*^{(2)}(z) &= c_1 z + \sum_{k=1}^{\infty} p_k z^{-k}, \\ \psi_*^{(2)}(z) &= c_2 z + \sum_{k=1}^{\infty} q_k z^{-k}, \quad (\text{with } c_1 = \sigma_y^\infty / 4, \quad (16) \\ & \quad c_2 = \sigma_y^\infty / 2) \end{aligned}$$

From Eqs. (11), (15) and (16), for the coefficients in Eq. (15) we have

$$a_1^{(2)} = R c_1 = \frac{R \sigma_y^\infty}{4}, \quad a_k^{(2)} = 0 \text{ for } k \geq 2 \quad (17)$$

$$b_1^{(2)} = R c_2 = \frac{R \sigma_y^\infty}{2}, \quad b_k^{(2)} = 0 \text{ for } k \geq 2 \quad (18)$$

From Eqs. (9) and (13), the traction free condition along the elliptic contour $z \in \Sigma_1$, or $\zeta \in \Gamma_1$ (or $\zeta = \rho_1 e^{i\theta}$ with $\rho_1 = 1$), is as follows

$$\phi^{(1)}(\zeta) + \frac{\omega(\zeta)}{\omega'(\zeta)} \overline{\phi^{(1)}(\zeta)} + \overline{\psi^{(1)}(\zeta)} = 0, \quad (19)$$

$$(\zeta = \rho_1 e^{i\theta}, \text{with } \rho_1 = 1)$$

The equality shown by Eq. (19) can be satisfied in a weaker form. To this end, we can perform the following operator

$$\frac{1}{2\pi i} \int_{\Gamma_1} [\dots] \zeta^{2j-2} d\zeta, \quad (j = -(N-1), \dots, 0, 1, \dots, N) \quad (20)$$

to both sides of Eq. (19). After taking this operation, we have

$$[\mathbf{F}_1]_{2N \times 4N} \{\mathbf{A}_1\}_{4N} = \{\mathbf{0}\}_{2N} \quad (21)$$

where

$$\{\mathbf{A}_1\}_{4N} = \{a_{-(N-1)}^{(1)} \dots a_0^{(1)} a_1^{(1)} \dots a_N^{(1)} b_{-(N-1)}^{(1)} \dots b_0^{(1)} b_1^{(1)} \dots b_N^{(1)}\}^T \quad (22)$$

The detail of performing the operator shown by Eq. (20) to both sides of Eq. (19) can be referred to (Chen 2015a).

In addition, the derivation for the matrix $[\mathbf{F}_1]_{2N \times 4N}$ can also be referred to some results in Appendix.

Now we consider the continuity condition for traction and displacement along the interface Σ_2 (Fig. 1). Since the resultant force function and the displacement should be continuous along the interface, from Eqs. (9), (10), (13) and (15) we have

$$\phi^{(1)}(\zeta) + \frac{\omega(\zeta)}{\omega'(\zeta)} \overline{\phi^{(1)}(\zeta)} + \overline{\psi^{(1)}(\zeta)} = \phi^{(2)}(\zeta) + \frac{\omega(\zeta)}{\omega'(\zeta)} \overline{\phi^{(2)}(\zeta)} + \overline{\psi^{(2)}(\zeta)}, \quad (23)$$

$$(\zeta \in \Gamma_2)$$

$$\frac{1}{G_1} \{\kappa_1 \phi^{(1)}(\zeta) - \frac{\omega(\zeta)}{\omega'(\zeta)} \overline{\phi^{(1)}(\zeta)} - \overline{\psi^{(1)}(\zeta)}\} = \frac{1}{G_2} \{\kappa_2 \phi^{(2)}(\zeta) - \frac{\omega(\zeta)}{\omega'(\zeta)} \overline{\phi^{(2)}(\zeta)} - \overline{\psi^{(2)}(\zeta)}\}, \quad (24)$$

$$(\zeta \in \Gamma_2)$$

It is seen that the continuation conditions shown by Eqs. (23) and (24) are expressed in the continuous form, which is formulated along the interface $\zeta \in \Gamma_2$ or $\zeta = \rho_2 e^{i\theta}$ (Fig. 1). Now we want to convert two conditions into a discrete form. To this end, we can perform the following operator

$$\frac{1}{2\pi i} \int_{\Gamma_2} [\dots] \zeta^{2j-2} d\zeta, \quad (j = -(N-1), \dots, 0, 1, \dots, N) \quad (25)$$

to both sides of Eqs. (23) and (24). After making the mentioned operation, from Eqs. (23) and (24) we will obtain the following transfer matrix relation as follows (Chen 2015a)

$$\{\mathbf{A}_1\}_{4N} = [\mathbf{K}_{12}]_{4N \times 4N} \{\mathbf{A}_2\}_{4N} \quad (26)$$

where the vector $\{\mathbf{A}_2\}_{4N}$ is defined by

$$\{\mathbf{A}_2\}_{4N} = \{a_{-(N-1)}^{(2)} \dots a_0^{(2)} a_1^{(2)} \dots a_N^{(2)} b_{-(N-1)}^{(2)} \dots b_0^{(2)} b_1^{(2)} \dots b_N^{(2)}\}^T \quad (27)$$

The matrix $[\mathbf{K}_{12}]_{4N \times 4N}$ is called the transfer matrix, which provides a relation between two vectors $\{\mathbf{A}_1\}_{4N}$ and $\{\mathbf{A}_2\}_{4N}$. For evaluating all elements in the matrix $[\mathbf{K}_{12}]_{4N \times 4N}$, we can refer to (Chen 2015a). In addition, the derivation for the matrix $[\mathbf{K}_{12}]_{4N \times 4N}$ can also be referred to some results in Appendix. The concept of the transfer matrix method can be referred to (Chen 2015a).

Substituting Eq. (26) into Eq. (21), we will find

$$[\mathbf{F}_2]_{2N \times 4N} \{\mathbf{A}_2\}_{4N} = \{\mathbf{0}\}_{2N} \quad (28)$$

where

$$[\mathbf{F}_2]_{2N \times 4N} = [\mathbf{F}_1]_{2N \times 4N} [\mathbf{K}_{12}]_{4N \times 4N} \quad (29)$$

Eq. (28) can be rewritten as

$$[\mathbf{F}_{2p}]_{2N \times 2N} \{\mathbf{A}_{2p}\}_{2N} + [\mathbf{F}_{2q}]_{2N \times 2N} \{\mathbf{A}_{2q}\}_{2N} = \{\mathbf{0}\}_{2N} \quad (30)$$

where

$$\{\mathbf{A}_{2p}\}_{2N} = \{a_{-(N-1)}^{(2)} \dots a_0^{(2)} b_{-(N-1)}^{(2)} \dots b_0^{(2)}\}^T \quad (31)$$

$$\{\mathbf{A}_{2q}\}_{2N} = \{a_1^{(2)} \dots a_N^{(2)} b_1^{(2)} \dots b_N^{(2)}\}^T \quad (32)$$

Note that the two matrices $[\mathbf{F}_{2p}]_{2N \times 2N}$ and $[\mathbf{F}_{2q}]_{2N \times 2N}$ are some portion of the matrix $[\mathbf{F}_2]_{2N \times 4N}$.

From Eqs. (17) and (18) we see that, the vector $\{\mathbf{A}_{2q}\}_{2N} = \{a_1^{(2)} \dots a_N^{(2)} b_1^{(2)} \dots b_N^{(2)}\}^T$ is known beforehand. Thus, from Eq. (30) we have

$$[\mathbf{F}_{2p}]_{2N \times 2N} \{\mathbf{A}_{2p}\}_{2N} = \{\mathbf{g}\}_{2N} \quad (33)$$

where

$$\{\mathbf{g}\}_{2N} = -[\mathbf{F}_{2q}]_{2N \times 2N} \{\mathbf{A}_{2q}\}_{2N} \quad (34)$$

Finally, from Eq. (33) we can get a solution for the vector $\{\mathbf{A}_{2p}\}_{2N}$. Since the vector $\{\mathbf{A}_{2q}\}_{2N}$ (see Eqs. (17) and (18)) is known beforehand. Thus, we can obtain the vector $\{\mathbf{A}_2\}_{4N}$ (composed of the vector $\{\mathbf{A}_{2p}\}_{2N}$ and $\{\mathbf{A}_{2q}\}_{2N}$). In addition, from Eq. (26) we can obtain the vector $\{\mathbf{A}_1\}_{4N}$. Finally, the assumed boundary value problem is solved.

In fact, after two vectors $\{\mathbf{A}_1\}_{4N}$ and $\{\mathbf{A}_2\}_{4N}$ are obtained, we can evaluate the stress components at any point.

Table 1 The non-dimensional stress concentration factors $h_1(b_1/a_1, \beta)$ for the σ_{yc} (stress at the crown point of the inner elliptic contour Σ_1 in Fig. 1) versus the remote loading $\sigma_y^\infty = p$ in the case of two phases with $G_2/G_1 = \beta$ (see Fig. 1 and Eq. (35))

$\beta =$	10	2	1	0.5	0.1
$b_1/a_1 =$					
0.25	1.362	5.466	9.000	13.884	32.294
0.50	0.757	3.042	5.000	7.673	17.462
0.75	0.558	2.239	3.667	5.585	12.363
1.00	0.459	1.839	3.000	4.534	9.755

2.3 Numerical examples in the infinite matrix case

Two numerical examples are carried out for the infinite matrix case. In addition, the mapping function shown by Eq. (11) is used in all examples.

Example 1

In the example, the case for two phases is considered (Fig. 1). The elastic constants for the inner layer and the matrix are denoted by G_1 , κ_1 and G_2 , κ_2 , respectively. $\kappa_1 = \kappa_2 = 1.8$ is assumed in the example.

The inner elliptic contour Σ_1 has a shape of ellipse with two semi-axes “ a_1 ” and “ b_1 ”, which is the mapping of the function $z = \omega(\zeta)$ for $\Gamma_1 (\zeta = \rho_1 e^{i\theta}, \rho_1 = 1$ in the ζ -plane). The interface Σ_2 has a shape of ellipse with two semi-axes “ a_2 ” and “ b_2 ”, which is the mapping of the function $z = \omega(\zeta)$ for $\Gamma_2 (\zeta = \rho_2 e^{i\theta}$ in the ζ -plane). In computation, $\rho_2 = 1.5$ is used. The remote loading is denoted by $\sigma_y^\infty = p$. In addition, $N=28$ is adopted in the series expansion for the complex potentials shown by Eqs. (13) and (15).

As stated previously, after two vectors $\{A_1\}_{4N}$ and $\{A_2\}_{4N}$ are obtained, we can evaluate the stress components at any point. For the limitation of space, we only compute a few of them.

In computation, we assume the following conditions: (1) $b_1/a_1 = 0.25, 0.5, 0.75, 1$ (2) $\rho_1 = 1, \rho_2 = 1.5$, (3) $G_2/G_1 = \beta = 10, 2, 1, 0.5$ and 0.1 , and (4) the remote loading $\sigma_y^\infty = p$ (Fig. 1). The stress component σ_{yc} at the crown point (at the crown point $x=a_1, y=0$ in Fig. 1) of the elliptic contour Σ_1 can be expressed as

$$\sigma_{yc} = h_1(b_1/a_1, \beta)p, \quad (\text{with } \beta = G_2/G_1) \quad (35)$$

The computed results for $h_1(b/a, \beta)$ are listed in Table 1.

The non-dimensional stress concentration factors (SCFs) $h_1(b_1/a_1, \beta)$ represent the influence of the remote loading $\sigma_y^\infty = p$ to σ_{yc} (stress at the crown point $x = a_1, y = 0$ in Fig. 1). From Table 1 we see that the ratio $\beta = G_2/G_1$ has a significant influence to the value of $h_1(b_1/a_1, \beta)$. For example, in the case $b_1/a_1 = 0.25$, we have $h_1(b_1/a_1, \beta) \big|_{\beta=10} = 1.362$, $h_1(b_1/a_1, \beta) \big|_{\beta=1} = 9.000$ and $h_1(b_1/a_1, \beta) \big|_{\beta=0.1} = 32.294$, respectively. That is to say the SCF will be rather higher (=32.294) for the weaker matrix $G_2/G_1 = \beta = 0.1$.

Note that in the case of $G_2/G_1 = \beta = 1$, we have a closed form solution as follows (Muskhelishvili 1963)

$$h_1(b_1/a_1, \beta) \big|_{\beta=1} = \frac{2a_1}{b_1} + 1 \quad (36)$$

In addition, the computed results $h_1(b_1/a_1, \beta) \big|_{\beta=1} = 9.000, 5.000, 3.667, 3.000$ for $b_1/a_1 = 0.25, 0.5, 0.75, 1.0$ coincide with the result from the closed form solution shown by Eq. (36).

As stated previously, all the distributions of stresses can be found from the suggested technique. In the case of $b_1/a_1 = 0.5$ and the remote loading $\sigma_y^\infty = p$, the computed results for σ_N , σ_{NT} and σ_T in the interior side and the exterior side of the interface Σ_2 ($z = \omega(\zeta) \in \Sigma_2, \zeta = \rho_2 e^{i\theta} \in \Gamma_2$ in Fig. 1) are denoted by

$$\sigma_N = f_{N, \text{in}}(\theta)p, \quad \sigma_{NT} = f_{NT, \text{in}}(\theta)p, \quad \sigma_T = f_{T, \text{in}}(\theta)p,$$

$$(\text{at point } x = R(\rho_2 + m/\rho_2)\cos\theta,$$

$$y = R(\rho_2 - m/\rho_2)\sin\theta \quad (37)$$

in the interior side of the interface Σ_2 in Fig. 1)

$$\sigma_N = f_{N, \text{ex}}(\theta)p, \quad \sigma_{NT} = f_{NT, \text{ex}}(\theta)p, \quad \sigma_T = f_{T, \text{ex}}(\theta)p,$$

$$(\text{at point } x = R(\rho_2 + m/\rho_2)\cos\theta,$$

$$y = R(\rho_2 - m/\rho_2)\sin\theta \quad (38)$$

in the exterior side of the interface Σ_2 in Fig. 1)

In the first part of computation, we assume : (1) $b_1/a_1 = 0.5$, (2) $\rho_1 = 1, \rho_2 = 1.5$, (3) $\beta = G_2/G_1 = 2$ and (4) the remote loading $\sigma_y^\infty = p$, the computed results for non-dimensional stresses $f_{N, \text{in}}(\theta), f_{NT, \text{in}}(\theta), f_{T, \text{in}}(\theta)$

and $f_{N,ex}(\theta)$, $f_{NT,ex}(\theta)$, $f_{T,ex}(\theta)$ along the interface Σ_2 are plotted in Fig. 2. From Fig. 2 we see that $f_{N,in}(\theta) = f_{N,ex}(\theta)$, $f_{NT,in}(\theta) = f_{NT,ex}(\theta)$. That is to say, the continuity conditions for the stress components σ_N and σ_{NT} along the interface are satisfied with higher accuracy in the numerical example. In addition, we find that $f_{T,in}(\theta) \neq f_{T,ex}(\theta)$. for example, $f_{T,in}(\theta)|_{\theta=180^\circ} = 1.293$, $f_{T,ex}(\theta)|_{\theta=180^\circ} = 2.396$, and $f_{T,in}(\theta)|_{\theta=180^\circ} < f_{T,ex}(\theta)|_{\theta=180^\circ}$.

In the second part of computation, we assume : (1) $b_1/a_1 = 0.5$, (2) $\rho_1 = 1$, $\rho_2 = 1.5$, (3) $\beta = G_2/G_1 = 0.5$ and (4) the remote loading $\sigma_y^\infty = p$, the computed results for non-dimensional stresses $f_{N,in}(\theta)$, $f_{NT,in}(\theta)$, $f_{T,in}(\theta)$ and $f_{N,ex}(\theta)$, $f_{NT,ex}(\theta)$, $f_{T,ex}(\theta)$ along the interface Σ_2 are plotted in Fig. 3. From Fig. 3 we see that $f_{N,in}(\theta) = f_{N,ex}(\theta)$, $f_{NT,in}(\theta) = f_{NT,ex}(\theta)$. That is to say, the continuity conditions for the stress components σ_N and σ_{NT} along the interface are satisfied with higher accuracy in the numerical example. In addition, we find that $f_{T,in}(\theta) \neq f_{T,ex}(\theta)$. for example, $f_{T,in}(\theta)|_{\theta=180^\circ} = 1.776$, $f_{T,ex}(\theta)|_{\theta=180^\circ} = 1.069$, and $f_{T,in}(\theta)|_{\theta=180^\circ} > f_{T,ex}(\theta)|_{\theta=180^\circ}$. This result (for $\beta = G_2/G_1 = 0.5$ with $f_{T,in}(\theta)|_{\theta=180^\circ} > f_{T,ex}(\theta)|_{\theta=180^\circ}$) is contrary to the result in the first part of computation (for $\beta = G_2/G_1 = 2$ with $f_{T,in}(\theta)|_{\theta=180^\circ} < f_{T,ex}(\theta)|_{\theta=180^\circ}$).

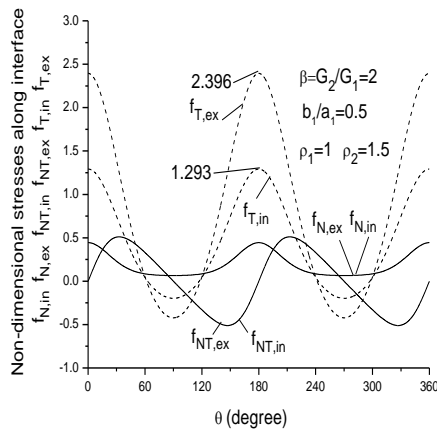


Fig. 2 Non-dimensional stresses $f_{N,in}(\theta)$, $f_{NT,in}(\theta)$, $f_{T,in}(\theta)$ (in the interior side of interface Σ_2), $f_{N,ex}(\theta)$, $f_{NT,ex}(\theta)$, $f_{T,ex}(\theta)$ (in the exterior side of interface Σ_2) in the case of (1) $b_1/a_1 = 0.5$, (2) $\rho_1 = 1$, $\rho_2 = 1.5$ (3) remote loading σ_y^∞ and (4) $\beta = G_2/G_1 = 2$ (see Fig. 1 and Eqs. (37) and (38))

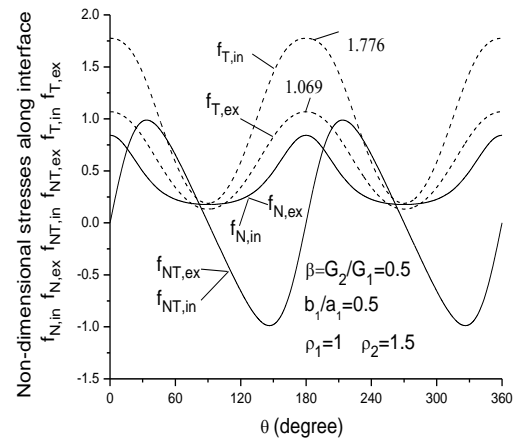


Fig. 3 Non-dimensional stresses $f_{N,in}(\theta)$, $f_{NT,in}(\theta)$, $f_{T,in}(\theta)$ (in the interior side of interface Σ_2), $f_{N,ex}(\theta)$, $f_{NT,ex}(\theta)$, $f_{T,ex}(\theta)$ (in the exterior side of interface Σ_2) in the case of (1) $b_1/a_1 = 0.5$, (2) $\rho_1 = 1$, $\rho_2 = 1.5$ (3) remote loading σ_y^∞ and (4) $\beta = G_2/G_1 = 0.5$ (see Fig. 1 and Eqs. (37) and (38))

Example 2

In the second example, all the geometry and loading conditions are the same as indicated in the first example (Fig. 4). The two portions have the same elastic properties, or G_1, G_2 (with $G_1 = G_2$) and $\kappa_1 = \kappa_2 = 1.8$. However, the thicknesses of two portions are different, or t_1, t_2 (with $t_1 \neq t_2$) (Fig. 4). A ratio is defined by $\gamma = t_1/t_2$.

Clearly, the proposed problem can be reduced to an alternative problem with different elastic properties, or G_1, G_2 (with $G_2 = G_1/\gamma$) and $\kappa_1 = \kappa_2 = 1.8$ and t_1, t_2 (with $t_1 = t_2$). Therefore, this problem is reduced to the problem proposed in the first example.

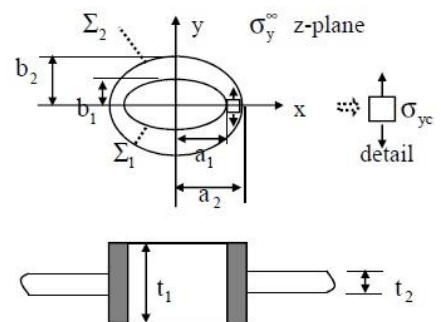


Fig. 4 A stiffening problem with thickness t_1 and t_2 for two portions (the elliptic layer bounded by Σ_1 and Σ_2 and the infinite matrix exterior to Σ_2)

Table 2 The non-dimensional stress concentration factors $h_2(b_1/a_1, \gamma)$ for the σ_{yc} (stress at the crown point $x = a_1, y = 0$ of the inner elliptic contour Σ_1) versus the remote loading $\sigma_y^\infty = p$ in the case of unequal thickness of two portions with $\gamma = t_1/t_2$ (see Fig. 4 and Eq. (39))

$\gamma =$	1	2	3	4	5	6	7	8	9	10
$b_1/a_1 =$										
0.25	9.000	6.942	5.826	5.104	4.590	4.198	3.886	3.630	3.415	3.229
0.5	5.000	3.836	3.204	2.797	2.507	2.287	2.112	1.969	1.849	1.746
0.75	3.667	2.792	2.317	2.013	1.797	1.634	1.505	1.400	1.312	1.236
1.0	3.000	2.267	1.869	1.615	1.436	1.301	1.195	1.109	1.037	0.976

In computation, we assume the following conditions:

- (1) $b_1/a_1 = 0.25, 0.5, 0.75, 1$, (2) $\rho_1 = 1, \rho_2 = 1.5$, (3) $t_1/t_2 = 1, 2, \dots, 10$ and (4) the remote loading $\sigma_y^\infty = p$.

The stress component σ_{yc} at the crown point (at the point $x = a_1, y = 0$ in Fig. 4) of the elliptic contour Σ_1 can be expressed as

$$\sigma_{yc} = h_2(b_1/a_1, \gamma)p, \quad (\text{with } \gamma = t_1/t_2) \quad (39)$$

The computed results for $h_2(b_1/a_1, \gamma)$ are listed in Table 2.

The non-dimensional stress concentration factors (SCFs) $h_2(b_1/a_1, \gamma)$ (with $\gamma = t_1/t_2$) represent the influence of the remote loading $\sigma_y^\infty = p$ to σ_{yc} (stress at the crown point in Fig. 4). From Table 2 we see that the ratio $\gamma = t_1/t_2$ has a significant influence to the value of $h_2(b_1/a_1, \gamma)$. For example, in the case $b_1/a_1 = 0.25$, we have $h_2(b_1/a_1, \gamma)|_{\gamma=1} = 9.000$, $h_2(b_1/a_1, \gamma)|_{\gamma=5} = 4.590$ and $h_2(b_1/a_1, \gamma)|_{\gamma=10} = 3.229$, respectively. That is to say the SCF will be rather lower (=3.229) for the thicker inner elliptic layer with $\gamma = t_1/t_2 = 10$.

3. Formulation of the problem in the finite matrix case

3.1 Derivation for the finite matrix case

It is assumed that the finite matrix layer is placed exterior to the contour Σ_2 (Fig. 5). The normal loading “q” is applied along the boundary Σ_3 , or the mapping of $\zeta = \rho_3 e^{i\theta}$ for $z = \omega(\zeta)$. The conformal mapping shown by Eq. (11) is still used in the present case. From this loading condition and Eq. (9), the boundary condition

along the elliptic contour Σ_3 will be

$$\phi^{(2)}(\zeta) + \frac{\omega(\zeta)}{\omega'(\zeta)} \overline{\phi^{(2)}(\zeta)} + \overline{\psi^{(2)}(\zeta)} = q\omega(\zeta) = qR(\zeta + \frac{m}{\zeta}), \quad (\zeta = \rho_3 e^{i\theta}) \quad (40)$$

Note that, those equations, from Eqs. (11) to (29), are still valid in the present case.

Now we want to convert the condition shown by Eq. (40) into a discrete form. To this end, we can perform the following operator

$$\frac{1}{2\pi i} \int_{\Gamma_3} [\dots] \zeta^{2j-2} d\zeta, \quad (j = -(N-1), \dots, 0, 1, \dots, N) \quad (41)$$

to both sides of Eq. (40). After taking this operation, we have

$$[\mathbf{F}_3]_{2N \times 4N} \{\mathbf{A}_2\}_{4N} = \{\mathbf{g}\}_{2N} \quad (42)$$

where

$$\{\mathbf{g}\}_{2N} = \{00 \dots qR \ m qR \ 0 \dots 0\}^T \quad (43)$$

From Eqs. (28) and (42) we can get the following linear algebraic equation for the vector $\{\mathbf{A}_2\}_{4N}$

$$[\mathbf{F}_s]_{4N \times 4N} \{\mathbf{A}_2\}_{4N} = \{\mathbf{h}\}_{4N} \quad (44)$$

where

$$[\mathbf{F}_s]_{4N \times 4N} = \begin{bmatrix} [\mathbf{F}_2]_{2N \times 4N} \\ [\mathbf{F}_3]_{2N \times 4N} \end{bmatrix}, \quad \{\mathbf{h}\}_{4N} = \begin{bmatrix} \{0\}_{2N} \\ \{\mathbf{g}\}_{2N} \end{bmatrix} \quad (45)$$

Finally, from Eq. (44) we can get a solution for the vector $\{\mathbf{A}_2\}_{4N}$. In addition, from Eq. (26) we can obtain the vector $\{\mathbf{A}_1\}_{4N}$. Finally, the assumed boundary value problem for the case of finite matrix is solved (Fig. 5).

3.2 Numerical example

In computation, we assume the following

conditions:(1) $b_1/a_1 = 0.25, 0.5, 0.75, 1$ (2), $\rho_1 = 1$, $\rho_2 = 1.5$, $\rho_3 = 3$, (3) $G_2/G_1 = \beta = 10, 2, 1, 0.5$ and 0.1 , and (4) the normal loading “q” is applied along the contour Σ_3 (Fig. 5). The stress component σ_{yc} at the crown point (at the point $x = a_1, y = 0$ in Fig. 5) of the elliptic contour Σ_1 can be expressed as

$$\sigma_{yc} = h_3(b_1/a_1, \beta)q \quad (\text{with } \beta = G_2/G_1) \quad (46)$$

The computed results for $h_3(b/a, \beta)$ are listed in Table 3.

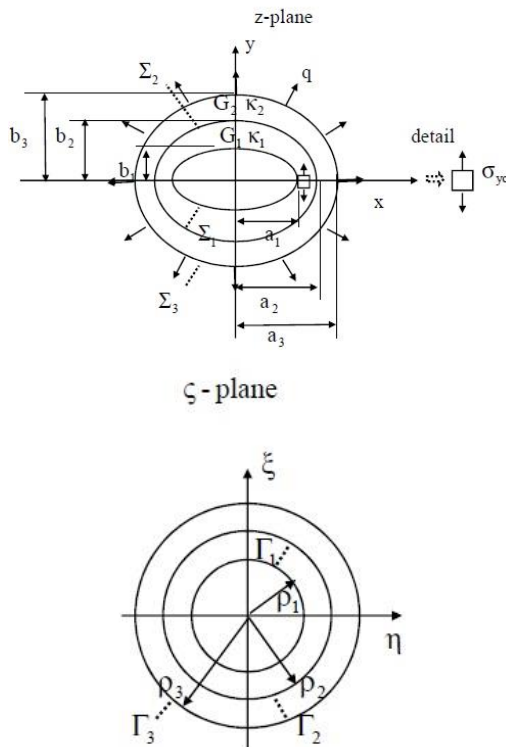


Fig. 5 Mapping relations: (1) the elliptic layer bounded by two ellipses Σ_1 (with two semi-axes “ a_1 ” and “ b_1 ”) and Σ_2 (with two semi-axes “ a_2 ” and “ b_2 ” and $\sqrt{a_2^2 - b_2^2} = \sqrt{a_1^2 - b_1^2}$), (in the z -plane) with elastic constants G_1, K_1 mapped into ring region bounded by two circles Γ_1 and Γ_2 , or $\rho_1 \leq |\zeta| \leq \rho_2$ with $\rho_1 = 1$ (in the ζ -plane), (2) the elliptic layer bounded by two ellipses Σ_2 (with two semi-axes “ a_2 ” and “ b_2 ”) and Σ_3 (with two semi-axes “ a_3 ” and “ b_3 ” and $\sqrt{a_1^2 - b_1^2} = \sqrt{a_2^2 - b_2^2} = \sqrt{a_3^2 - b_3^2}$), (in the z -plane) with elastic constants G_2, K_2 mapped into ring region bounded by two circles Γ_2 and Γ_3 , or $\rho_2 \leq |\zeta| \leq \rho_3$ (in the ζ -plane)

Table 3 The non-dimensional stress concentration factors $h_3(b_1/a_1, \beta)$ for the σ_{yc} (stress at the crown point of the inner elliptic contour Σ_1) versus the loading “q” in the case of two phases with $G_2/G_1 = \beta$, $\rho_1 = 1$, $\rho_2 = 1.5$ and $\rho_3 = 3$ (see Fig. 5 and Eq. (46))

$\beta =$	10	2	1	0.5	0.1
$b_1/a_1 =$					
0.25	2.375	8.314	12.705	18.229	35.699
0.50	1.056	3.743	5.700	8.049	14.742
0.75	0.621	2.240	3.396	4.690	7.695
1.00	0.403	1.491	2.250	3.018	4.152

The non-dimensional stress concentration factors (SCFs) $h_3(b_1/a_1, \beta)$ represent the influence of the normal loading “q” along Σ_3 to σ_{yc} (the stress at the crown point, $x = a_1, y = 0$, in Fig. 5). From Table 3 we see that the ratio $\beta = G_2/G_1$ has a significant influence to the value of $h_3(b_1/a_1, \beta)$. For example, in the case $b_1/a_1 = 0.25$, we have $h_3(b_1/a_1, \beta)|_{\beta=10} = 2.375$, $h_3(b_1/a_1, \beta)|_{\beta=1} = 12.705$ and $h_3(b_1/a_1, \beta)|_{\beta=0.1} = 35.699$, respectively. That is to say the SCF will be rather higher (35.699) for the weaker matrix $G_2/G_1 = \beta = 0.1$.

4. Conclusions

This paper provides an effective method to solve a rather complicated problem, or the problem for the stress analysis for multiple confocal elliptic dissimilar cylinders. It is an important step to satisfy the boundary condition and the continuity conditions shown by Eqs. (19), (23), (24) and (40) in a weaker form.

References

Chen, J.T. and Wu, A.C. (2007), “Null-field approach for the multi-inclusion problem under antiplane shears”, *J. Appl. Mech.*, **74**(3), 469-487.
 Chen, T. (2004), “A confocally multicoated elliptical inclusion under antiplane shear: some new results”, *J. Elas.*, **74**(1), 87-97.
 Chen, Y.Z. (2013), “Closed-form solution for Eshelby’s elliptic inclusion in antiplane elasticity using complex variable”, *Z. Angew. Math. Phys.*, **64**(6), 1797-1805.
 Chen, Y.Z. (2015a), “Transfer matrix method for the solution of multiple elliptic layers with different elastic properties. Part I: infinite matrix case”, *Acta Mech.*, **226**(1), 191-209.
 Chen, Y.Z. (2015b), “A novel solution for thick-walled cylinders made of functionally graded materials”, *Smart Struct. Syst.*, **15**(6), 1503-1520.
 Gong, S.X. (1995), “A unified treatment of the elastic elliptical

inclusion under antiplane shear”, *Arch. Appl. Mech.*, **65**(2), 55-64.
 Markenscoff, X. and Dundurs, J. (2014), “Annular inhomogeneities with eigenstrain and interphase modeling”, *J. Mech. Phys. Solids*, **64**, 468-482.
 Muskhelishvili, N.I. (1963), *Some Basic Problems of the Mathematical Theory of Elasticity*. Noordhoff, Groningen.
 Wang, X. and Gao, X.L. (2011), “On the uniform stress state inside an inclusion of arbitrary shape in a three-phase composite”, *Z. Angew. Math. Phys.*, **62**(6), 1101-1116.
 Wu, C.H. and Chen, C.H. (1990), “A crack in a confocal elliptic inhomogeneity embedded in an infinite medium”, *J. Appl. Mech.*, **57**(1), 91-96.
 Zhu, L., Hoh, H.J., Wang, X., Keer, L.M., Pang, J.H.L., Song, B. and Wang, Q.J. (2013), “A review of recent works on inclusions”, *Mech. Mater.*, **60**, 144-158.

CC

Appendix. Some integrations used in the derivation

First of all, we define two particular integrals as follows

$$I_1 = \frac{1}{2\pi i} \int_{\Gamma} \zeta^{n-1} d\zeta, \quad (n- \text{integer}) \quad (a1)$$

$$I_2 = \frac{1}{2\pi i} \int_{\Gamma} \frac{\zeta^n}{\zeta^2 - q^2} d\zeta, \quad (n- \text{integer}) \quad (a2)$$

where Γ denotes a circle with radius ρ and “q” is a positive real value with property $q > \rho$ (Fig. 6).

Clearly, we have

$$I_1 = \frac{1}{2\pi i} \int_{\Gamma_1} \zeta^{n-1} d\zeta = \delta_n \quad (a3)$$

where

$$\delta_n = 1 \quad \text{for } n=0, \quad \text{and } \delta_n = 0 \quad \text{for } n \neq 0 \quad (a4)$$

In addition, we can obtain the following result (Chen 2015a)

$$I_2 = \frac{1}{2\pi i} \int_{\Gamma} \frac{\zeta^n}{\zeta^2 - q^2} d\zeta = \frac{1}{2\pi i} \int_{\Gamma} \frac{1}{2q} \left(\frac{1}{\zeta - q} - \frac{1}{\zeta + q} \right) \zeta^n d\zeta = s_n(q) \Delta_n \quad (a5)$$

where

$$s_n(q) = -\frac{1 - (-1)^n}{2} q^{n-1} \quad (a6)$$

$$\Delta_n = 1 \quad \text{for } n \leq -1, \quad \text{and } \Delta_n = 0 \quad \text{for } n \geq 0 \quad (a7)$$

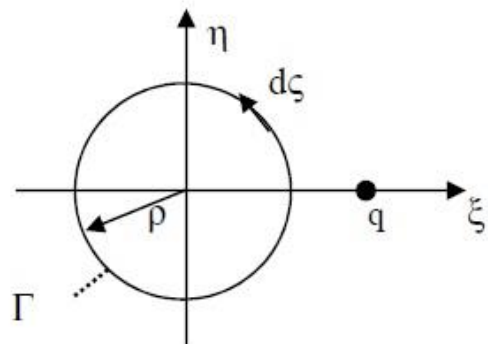


Fig. 6 A path Γ for integration